RESEARCH ARTICLE

WILEY

Global desertification vulnerability to climate change and human activities

Jianping Huang[1,2] | Guolong Zhang[2] | Yanting Zhang[3] | Xiaodan Guan[1,2] | Yun Wei[2] | Ruixia Guo[4]

[1]Collaborative Innovation Center for Western Ecological Safety, Lanzhou University, Lanzhou, China

[2]College of Atmospheric Sciences, Lanzhou University, Lanzhou, China

[3]Center for Monsoon System Research, Institute of Atmospheric Physics, Chinese Academy of Sciences, Beijing, China

[4]Key Laboratory of Land Surface Process and Climate Change in Cold and Arid Regions, Northwest Institute of Eco-Environment and Resources, Chinese Academy of Sciences, Lanzhou, China

Correspondence
Jianping Huang, Collaborative Innovation Center for Western Ecological Safety, Lanzhou University, 222 Tianshui South Road, Lanzhou, Gansu 730000, PR, China.
Email: hjp@lzu.edu.cn

Funding information
Fundamental Research Funds for the Central Universities, Grant/Award Numbers: lzujbky-2019-kb02, lzujbky-2019-kb30; National Natural Science Foundation of China, Grant/Award Numbers: 41521004, 41991231; The China 111 Project, Grant/Award Number: B13045; the Second Tibetan Plateau Scientific Expedition and Research Program, Grant/Award Number: 2019QZKK0602

Abstract

Desertification is the impoverishment of arid, semiarid, and some subhumid ecosystems. The assessment of global scale desertification vulnerability to climate change and human activity is important to help decision makers formulate the best strategies for land rehabilitation and combat global desertification in sensitive areas. There is no global desertification vulnerability map that considers both climate change and human activities. The main aim of this study was to construct a new index, the global desertification vulnerability index (GDVI), by combining climate change and human activity, provide another perspective on desertification vulnerability on a global scale, and project its future evolution. Using the probability density function of the GDVI, we classified desertification vulnerability into four classes: very high, high, medium, and low. The results of the analysis indicated that areas around deserts and barren land have a higher risk of desertification. Areas with a moderate, high, and very high desertification risk accounted for 13%, 7%, and 9% of the global area, respectively. Among the representative concentration pathways (RCPs), RCP8.5 projected that the area of moderate to very high desertification risk will increase by 23% by the end of this century. The areas where desertification risks are predicted to increase over time are mainly in Africa, North America, and the northern areas of China and India.

KEYWORDS

climate change, desertification, dryland, human activities, vulnerability index

1 | INTRODUCTION

The United Nations Convention to Combat Desertification (UNCCD) defines desertification (UNCCD, 1994) as "land degradation in arid, semiarid, and dry sub-humid areas resulting from various factors, including climatic variation and human activities." Human activities such as pollution, the exploitation of natural land for agriculture, and overgrazing are the main factors triggering desertification and land degradation (Brandt & Thornes, 1996; Yassoglou & Kosmas, 2000; Geist & Lambin, 2004; Yu et al., 2018). Climate change triggers desertification (Nicholson, 2002) by altering the spatiotemporal patterns in temperature, rainfall, and wind (Sivakumar, 2007). Desertification is a serious threat to arid and semiarid environments, which cover about 41% of the global land area and are home to more than 38% of the total global population (Global Land Project, 2005; Huang et al., 2017). It has been reported that desertification affects one quarter of the world's land surface, and 10–20% of drylands are already degraded (medium certainty; Millennium Ecosystem Assessment, 2005; UNCCD, 1994), which directly affects some 250 million people in the developing world. This figure is likely to expand substantially in the face of climate change and population growth (PG; Reynolds et al., 2007; Huang et al., 2016, 2017, 2019).

The identification and projection of areas that are vulnerable to desertification would enable policymakers to develop the best

strategies for slowing down desertification and establishing suitable land rehabilitation projects in sensitive areas. However, desertification is a complex phenomenon that is usually promoted by multiple causal agents (Geist & Lambin, 2004; Qi et al., 2013), such as biophysical and socioeconomic factors (Stafford Smith & Reynolds, 2002; Verstraete et al., 2009; Jafari & Bakhshandehmehr, 2016). Many mathematical models have been developed to delineate areas of desertification vulnerability on the basis of different indexes and data sets. The most frequently applied is the Mediterranean Desertification and Land Use Model, which incorporates the four main land degradation and desertification factors—climate, soil, vegetation, and land management—into an environmental sensitivity index to map the environmental sensitivity to desertification (Kosmas et al., 1999; Lavado Contador et al., 2009). However, the Mediterranean Desertification and Land Use model needs to be modified when applied to other regions in order to consider special factors (Pravalie et al., 2017). Consequently, most studies have focused on the extent of regional desertification, and because the factors considered were different, these assessments are not able to be directly compared. The US Department of Agriculture (USDA) first provided a global desertification vulnerability on the basis of a reclassification of the Global Soil climate map and Global Soil map (Eswaran & Reich, 2003). Spinoni et al. (2015) assessed the global desertification risk considering only climate change. With the increasing use of satellites to monitor the Earth, abundant biophysical data are available on a global scale, such as the Leaf Area Index (LAI), which is an important factor of net primary production (NPP), water and nutrient use, and carbon balance. The number of data sets that describe social variables at global scales has also increased, such as population density (PD) data, carbon dioxide (CO_2) emissions, and gross domestic product (GDP) data. PD indicates the demand intensity of human activities for natural resources, which imposes a direct pressure on the environment. Both CO_2 emissions and GDP represent the economic and development status. With increasingly global data sets available, the *World Atlas of Desertification*, third edition (Cherlet et al., 2018), suggested exploring and combining a variety of different global data sets. However, no uniform index that considers both human activities and climate change is suitable for assessing global desertification vulnerability. Although some studies have explored future desertification vulnerability using different methods (Henderson-Sellers et al., 2008; Miao et al., 2015; Rampone & Valente, 2019), the global desertification vulnerability to climate change and human activities has been largely ignored. The Fifth Coupled Model Intercomparison Project (CMIP5) has generated projections under different emission scenarios and could provide the data necessary for projecting desertification vulnerability. Therefore, the main aims of this study are to (a) construct a new index, the Global Desertification Vulnerability Index (GDVI), by combining climate change and human activity on a global scale, and to (b) assess the spatiotemporal evolution of global desertification from 2000 to 2014 and (c) project future global desertification vulnerability by the end of this century under different scenarios.

2 | MATERIALS AND METHODS

2.1 | Data

PD, CO_2 emissions, GDP, surface air temperature anomaly, aridity index (AI), and LAI data were used to construct GDVI, as shown in Figure 1. The PD, CO_2 emissions, and GDP were used to build the human activity index (HAI). NPP and soil moisture were used to validate the GDVI. We used the Food and Agriculture Organization of the United Nations definition of AI, in which AI is defined as the ratio of the annual precipitation to the annual potential evapotranspiration (Food and Agriculture Organization of the United Nations, 1977). Anomaly means a departure from a reference value or long-term average; here, surface air temperature anomaly (ΔT) refers to the departure of surface air temperature from the mean temperature during the period 1961–1990 at each pixel for the given year. All of the data sets have different spatial resolutions. To make them compatible, we interpolated the data to a resolution of $1.0° \times 1.0°$. Because different data sets have different temporal resolutions, all data sets were calculated to an annual mean. Additionally, some of the data sets had a different time length; thus, 2000–2014 was chosen to represent the observation period, and 2015–2100 was used for future projections. Given the different magnitudes of the data sets, we used the 99.9% and 0.1% thresholds as the maximum and minimum values to rescale the data between 0 and 1 when constructing GDVI. Thus LAI, AI, ΔT, and HAI have the same spatiotemporal resolution and magnitude. Twenty CMIP5 models (Table S1) were used to analyze the future changes of GDVI. Two future scenario predictions from 2006 to 2100 with medium (representative concentration pathway 4.5 [RCP4.5]) and high (RCP8.5) greenhouse gas emissions were conducted. We used the multimodel ensemble mean to reduce the uncertainty in future projections. More detailed information about data sets source and description are found in the Supporting Information.
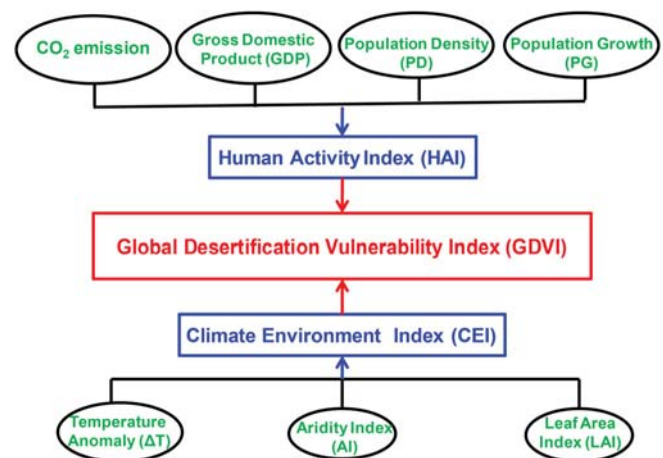

FIGURE 1 Diagram of the global desertification vulnerability index (GDVI) [Colour figure can be viewed at wileyonlinelibrary.com]
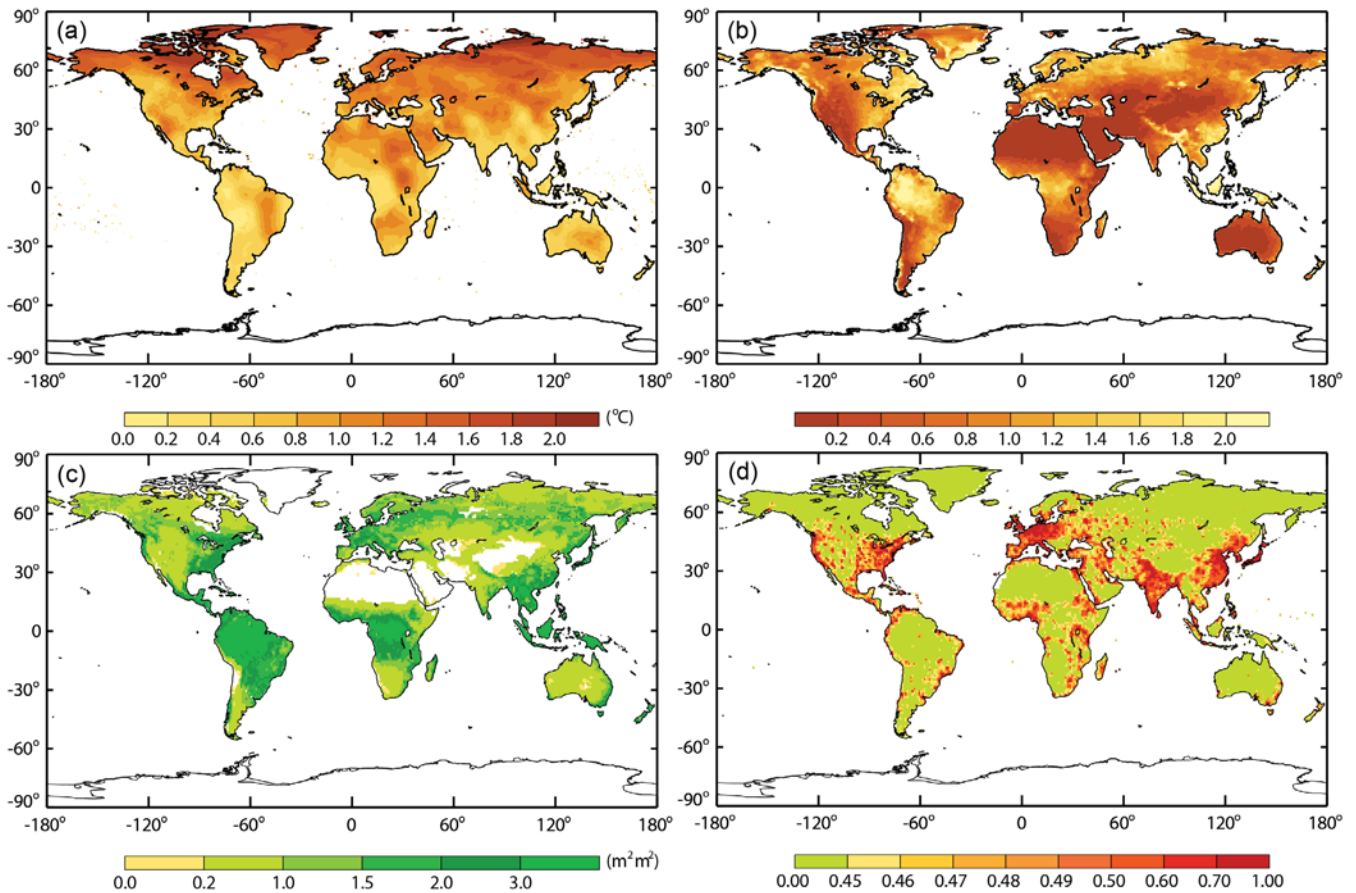
FIGURE 2 Global Distribution of the Mean (a) Surface Air Temperature Anomaly (ΔT), (b) Aridity Index, (c) Leaf Area Index, and (d) Human Activity Index for 2000–2014 [Colour figure can be viewed at wileyonlinelibrary.com]

2.2 | Methods

2.2.1 | Estimation of the HAI

To estimate the influence of human activity, we constructed an HAI on the basis of four human indicators: PD, PG, CO_2 emissions, and GDP (Zhang et al., 2017). The larger PD indicates that more natural resources are required and more pressure is imposed on the environment. PG is the result of the impact of social policy on population, with an increase in population implying more pressure on the environment over time. CO_2 emissions and GDP are indicators of the current economic and development status. The HAI was defined as follows:

$$HAI = w_1 PD(t) + w_2 PG(t) + w_3 CO_2(t) + w_4 GDP(t), \qquad (1)$$

where w_1, w_2, w_3, and w_4 are the weighting coefficients of PD, PG, CO_2 emissions, and GDP, respectively, as determined by the criteria importance obtained through the intercriteria correlation (CRITIC) method (Diakoulaki et al., 1995). PG in year i was defined as the difference in PD between year i and year $i – 1$.

$$PG_i = PD_i - PD_{i-1}. \qquad (2)$$

All four human activity indicators were nondimensionalized prior to constructing the HAI.

We normalized the HAI in the study using the following method:

$$x' = \begin{cases} 0 & (x < a) \\ \dfrac{x-a}{b-a} & (a \le x \le b), \\ 1 & (x > b) \end{cases} \qquad (3)$$

where x represents HAI, $a = \bar{x} - 2 \times \sigma$, $b = \bar{x} + 2 \times \sigma$, $\bar{x}$ is the mean of HAI, and σ is the standard deviation of HAI. The HAI ranges from 0 to 1 following normalization. A higher HAI implies greater human activity, suggesting a larger demand for natural resources and a greater possibility of land and water resource abuse (e.g., land overdevelopment, water shortages, and grassland overgrazing). Therefore, a higher HAI suggests a larger contribution of human activity to the desertification risk.

2.2.2 | Estimation of the GDVI

The GDVI was based on the assumption that the desertification risk is higher in areas with a high warming rate, high aridity, low vegetation
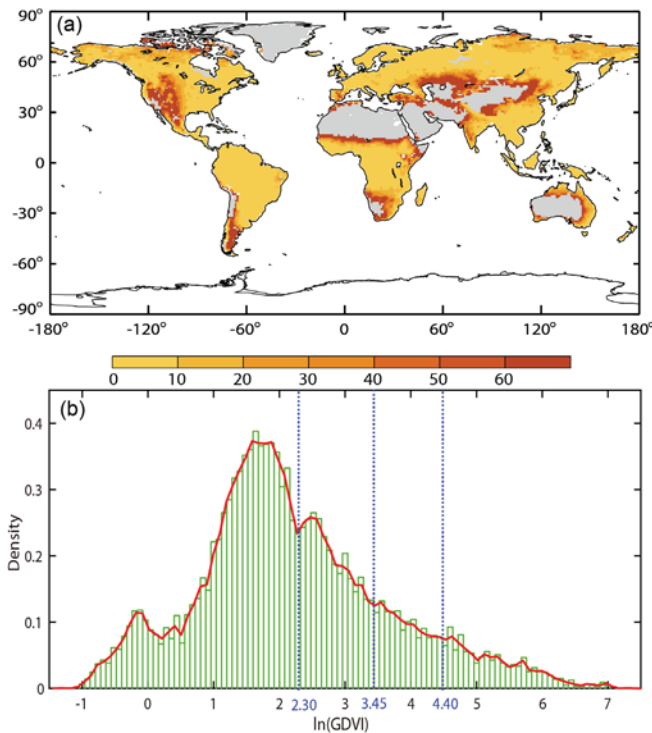
FIGURE 3 (a) Global distribution of the mean global desertification vulnerability index (GDVI) for 2000–2014. Areas dominated by barren land are shown in grey. (b) The probability density function for the logarithm of the GDVI. The blue dotted line represents the threshold value used to classify the GDVI [Colour figure can be viewed at wileyonlinelibrary.com]

cover, and intense human activity. We combined LAI, ΔT, AI, and HAI to construct GDVI. The GDVI values for each grid over the globe were obtained using the following formula:

$$GDVI = CEI \times HAI, \qquad (4)$$

where CEI = $1/LAI \times \Delta T/AI$, and CEI is the climate environment index.

Because the HAI was nondimensional and ranges from 0 to 1, ΔT, LAI, and AI were rescaled using Equation (5).

$$x' = \frac{x - x_{min}}{x_{max} - x_{min}}, \qquad (5)$$

where x represents ΔT, LAI, and AI. x_{max} and x_{min} are their maximum and minimum values, respectively, which were defined by the 99.9% and 0.1% thresholds. The type of indicator used to assess desertification vulnerability provided an overview of the evolution of ecosystems and environments.

2.2.3 | Statistical analysis

To give an intuitive view of global desertification vulnerability to climate change and human activities, we used a probability density distribution function to grade desertification vulnerability, estimated with our GDVI, into four classes: low, moderate, high, and very high. To verify the grading results, we compared our results with the desertification vulnerability map of USDA (Eswaran & Reich, 2003). First, because the USDA desertification vulnerability map data are rasterized on a 2-min grid cell, these data were aggregated into 1° spatial resolution data to match the GDVI data using the majority algorithm, which calculates the most prevalent desertification risk class for a 1° grid cell. Then we compared the spatial distribution of global vulnerability of our results and those of the USDA. We also calculated the area fraction of different subtypes estimated by the USDA and GDVI. Moreover, we calculated the Pearson correlation coefficients between GDVI, NPP, and soil moisture to test the reliability of the GDVI data at each pixel. The significance of the correlation was tested using Student's t test at the $p < .05$ level. To ensure the reliability of the future projection, we compared the results of a CMIP5-EM simulation with observations taken over the same period. To do this, bilinear interpolation was used to interpolate the spatial resolution results of the CMIP5 models into a 1° × 1° spatial resolution. In calculating the global-averaged HAI and LAI in Figure 9, each pixel was weighted using W_i [$W_i = \cos(\theta_i \times \pi/180.0)$, where θ_i is the latitude of grid i]. All of the maps and plots in Figures 2–11 were produced using National Center for Atmospheric Research Command Language Version 6.5.0. The function, "gsn_csm_contour_map," provided by the National Center for Atmospheric Research Command Language was used to produce the maps in Figures 2–11. That function could create and draw a contour plot over a map on the given workstation (https://www.ncl.ucar.edu/Document/Graphics/Interfaces/gsn_csm_contour_map.shtml). The attribute of map was added and modified by using MapPlot and MapTransformation (https://www.ncl.ucar.edu/Document/Graphics/Resources/mp.shtml#mpProjection). The coastlines of the map are the simplified version of those in the Regionally Accessible Nested Global Shorelines database, which was developed by Rainer Feistel from Wessel and Smith's Global Self-consistent Hierarchical High-resolution Shoreline database.

3 | RESULTS

3.1 | Global distribution of desertification vulnerability

The distribution of the mean ΔT, AI, LAI, and HAI from 2000 to 2014 were shown in Figure 2. It shows an increase in surface air temperature over the global continent, but with a nonuniform warming distribution (Figure 2a). The temperature warming in the Northern Hemisphere is significantly greater than that in the Southern Hemisphere, especially in some regions in the high latitudes, with the warming anomaly being greater than 2.0°C. Drylands occupy a large proportion of the global land area (Figure 2b), and therefore, desertification occurring in drylands may have a serious impact on human society and survival. The LAI is inversely correlated with the AI (Figure 2c). Vegetation in arid regions (e.g., northwestern China,
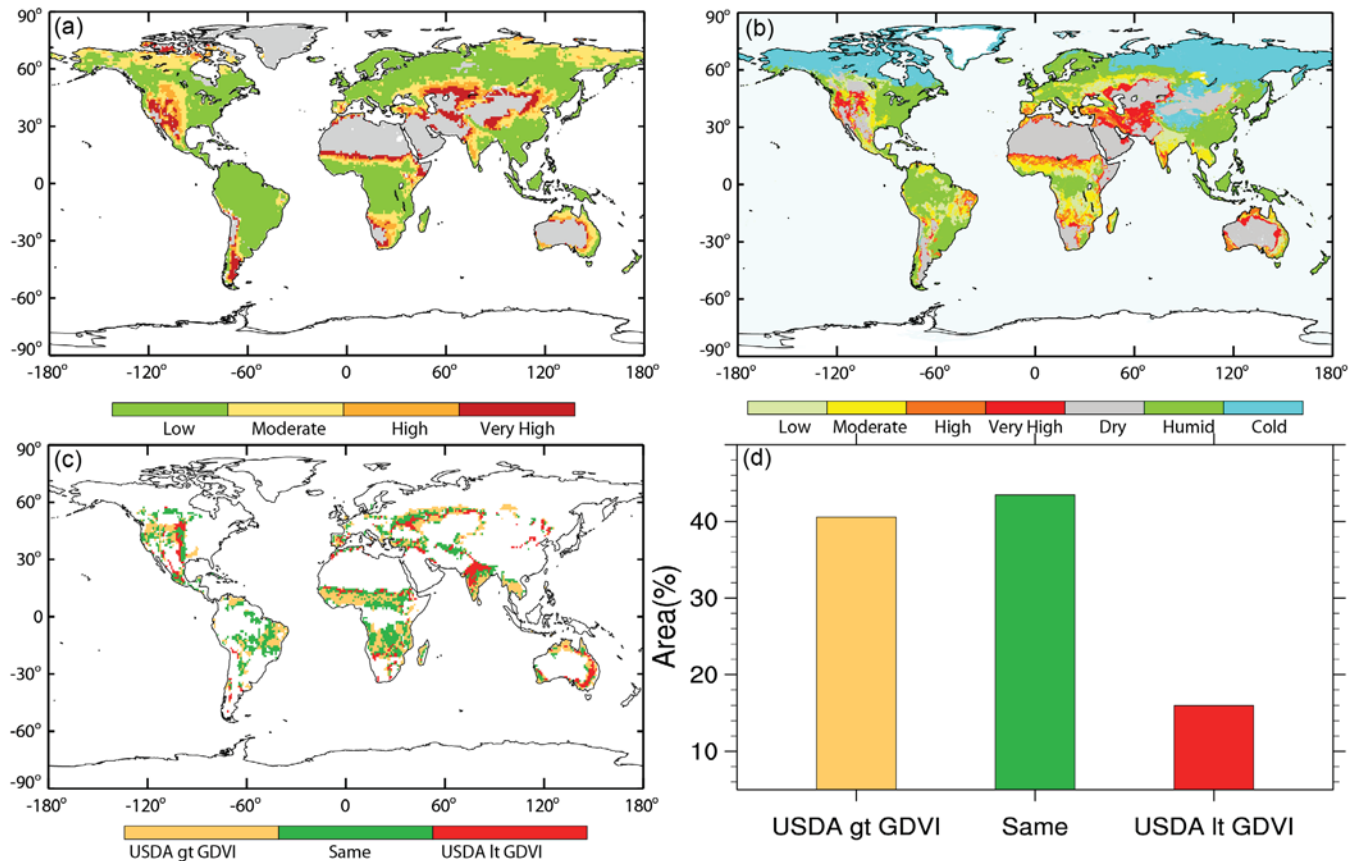
FIGURE 4 (a) The global distribution of desertification risk in the global desertification vulnerability index (GDVI) for 2000–2014 and (b) U.S. Department of Agriculture (USDA) data. (c) The global distribution of difference between GDVI with USDA data; (d) the area fraction of different risk occupy region was estimated by both two data. 'USDA gt GDVI' indicates that the level of USDA is higher than GDVI's, 'USDA lt GDVI' indicates that the level of USDA is lower than GDVI's, and 'Same' indicates that level of two data is coincident [Colour figure can be viewed at wileyonlinelibrary.com]

southern Africa, and Australia) is barren and sparse and must survive in a harsh living environment, with limited soil and water availability. In contrast, the vegetation cover is dense in humid regions, where the water supplied by precipitation is adequate and exceeds the losses due to evaporation. Figure 2d shows the distribution of the HAI. It shows that human activity is greatest in India, followed by the east of Asia, America, and central Africa, where the PD and CO_2 emissions are high.

On the basis of the CEI and HAI, the GDVI was estimated, and values were shown in Figure 3. We classified desertification vulnerability into four classes: very high (GDVI > 81.5), high (31.5 < GDVI ≤ 81.5), medium (10.0 < GDVI ≤ 31.5), and low (GDVI ≤ 10.0) according to the probability density function. There are two distinct peaks in the probability density function for the logarithm of GDVI, as shown in Figure 3b, where the logarithm of GDVI is 1.70 (GDVI = 5.5) and 2.50 (GDVI = 12.2), respectively. The local minimum, where the logarithm of GDVI is 2.3 (GDVI = 10.0), between two peaks is the point that determined the boundary between the low and medium classes. After the probability density reaches the second peak, it decreases rapidly to the point where the logarithm of GDVI is 3.45 (GDVI = 31.5) and then decreases slowly until the point where the logarithm of GDVI is 4.40 (GDVI = 81.5). The region where the

GDVI is greater than 31.5 and less than 81.5 is a transition region, in which desertification vulnerability was determined to be high, whereas to the right it is very high and to the left it is medium.

Figure 4a shows the mean GDVI distribution for 2000 to 2014. The high level of desertification risk is mainly in the western part of the United States, the Sahel, central Asia, and northern China, where vegetation is sparse (Figure 2c) and the climate is dry (Figure 2b). The desertification risk is moderate to severe in the Indian subcontinent and North China Plain due to intense human activity (Figure 2d). In southwestern Europe, the desertification risk is also moderate, which is consistent with previous studies (Martínez-Valderrama et al., 2016; Symeonakis et al., 2016).

We compared our results with the desertification vulnerability map made by the USDA (Eswaran & Reich, 2003). Regions with a humid, hyperarid, or cold climate are excluded, following the UNCCD definition of desertification. The spatial distribution of USDA data is similar to that of the GDVI data (Figure 4a,b). The area where two data are coincident dominates the distribution pattern (Figure 4c), mainly in Africa and South America. The most inconsistent region is in India and Indo-China Peninsula. In India, the risk is overestimated because of the intensive human activity. After considering the PD, it is determined that the Indian subcontinent had a high risk of
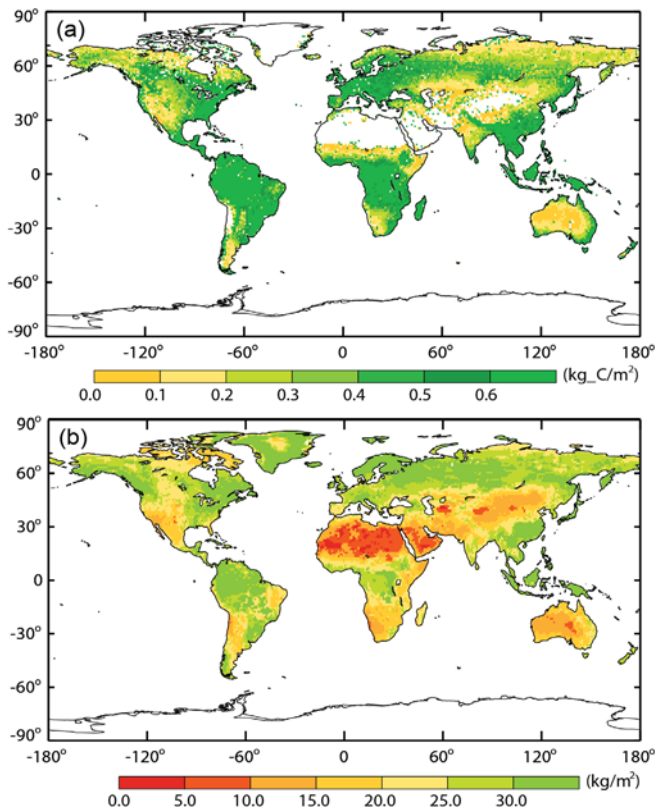
FIGURE 5 Global distribution of mean (a) net primary productivity and (b) soil moisture content for 2000–2014 [Colour figure can be viewed at wileyonlinelibrary.com]

FIGURE 6 (a) Frequency of certain net primary productivity (NPP) values for regions with different global desertification vulnerability index (GDVI) values for 2000–2014. (b) Distribution of the correlation coefficients for the relationship between NPP and GDVI. The stippling pattern indicates the 95% confidence level according to a two-tailed Student's *t* test [Colour figure can be viewed at wileyonlinelibrary.com]

desertification on the basis of USDA data (Eswaran et al., 2009). However, because of the high LAI, the desertification vulnerability is underestimated in the Indo-China Peninsula, where the GDVI is low. Because the USDA map was based on a reclassification of the global soil climate map and the global soil map, which are different components with those used in the GDVI, the two maps could not be coincided by point to point. Generally speaking, GDVI is reasonable and reliable.

To test how effective the GDVI is in assessing the desertification vulnerability, we compared the GDVI with NPP and soil moisture because NPP and soil moisture can be used to estimate the productivity of land and ecosystems over a region (Higginbottom & Symeonakis, 2014; Shinoda & Nandintsetseg, 2011). Desertification results in a reduction or loss of productivity in drylands. Therefore, NPP and soil moisture have a close relationship with desertification, with a higher desertification risk implying a smaller NPP. Figure 5 shows the global distribution of mean NPP and soil moisture for the period of 2000–2014. They show a similar distribution pattern, with a higher soil moisture content corresponding to a higher NPP. In barren regions, the soil moisture content is less than 15 kg m^{-2}, whereas in some extremely dry regions, it is less than 5 kg m^{-2} and the NPP is 0. Both NPP and soil moisture show the opposite distribution to that of the GDVI. Regions with a higher GDVI have a smaller NPP and soil moisture content (Figure 5a).
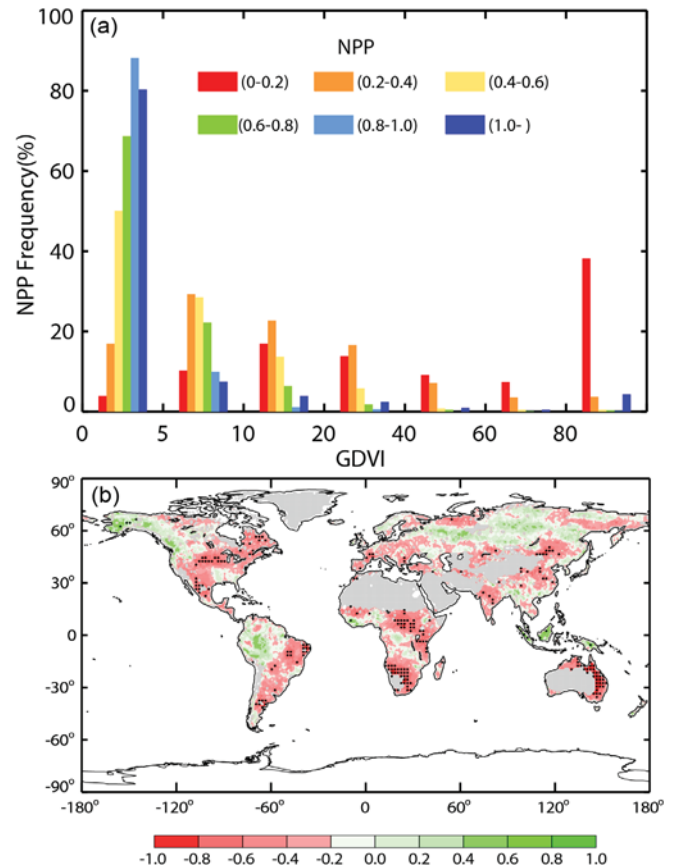
Figure 6a shows the frequency of certain NPP values for regions with different GDVI values. It shows that the regions with a high NPP are mainly located in regions with a lower GDVI, and the frequency of high NPP values decreases as the GDVI values increase. Regions where the high frequency of NPP values is 0–0.2 are mainly located in regions with a GDVI greater than 80. This confirmed that the GDVI has a close relationship with biological productivity. Regions with a lower level of vegetation productivity are more sensitive to climate change and human activity and thus more vulnerable to desertification (Le Houérou 1996; Reynolds et al., 2007; Lavado Contador et al., 2009). NPP and GDVI have a negative correlation in most regions, except the very cold high latitudes where there is extensive snow and ice cover (Figure 6b). The negative correlation coefficient indicated that regions with a high desertification risk has a low NPP. Over the high latitudes, there is a positive relationship between NPP and GDVI. This may be because there are large areas of ice and snow over these regions, with little vegetation cover. When temperature increases over these regions, the ice and snow may melt, and the environment will become more suitable for the growth of vegetation.
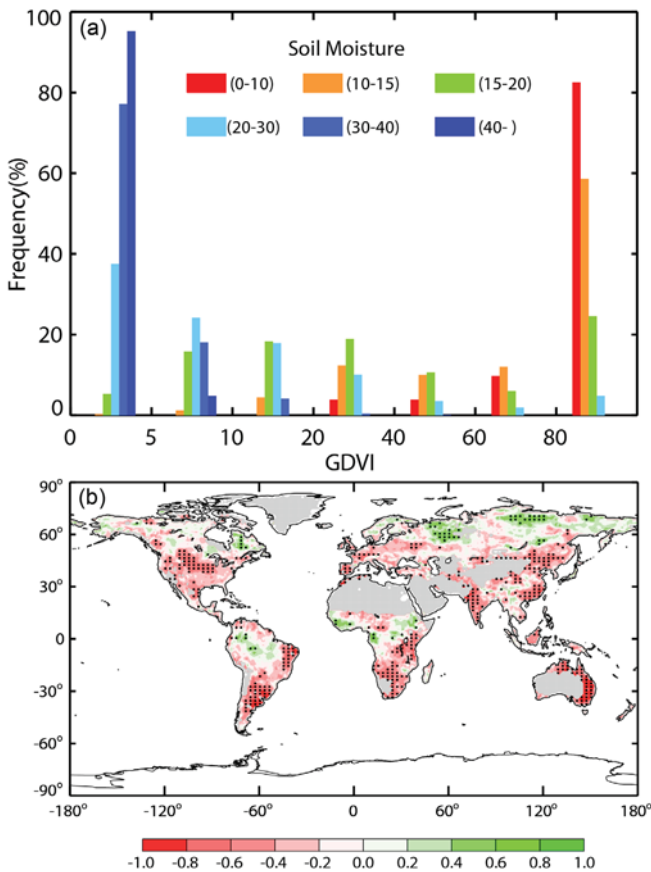
FIGURE 7 (a) Frequency of certain soil moisture values for regions with different global desertification vulnerability index (GDVI) values for 2000–2014. (b) Distribution of the correlation coefficients for the relationship between soil moisture and GDVI. The stippling pattern indicates the 95% confidence level according to a two-tailed Student's t test [Colour figure can be viewed at wileyonlinelibrary.com]

This contradicts our previous assumption that the desertification risk is higher in areas with high temperatures.

The relationship between soil moisture and GDVI is shown in Figure 7. Soil moisture content larger than 30 kg m^{-2} is mainly in regions with GDVI less than 20. Soil moisture content less than 15 kg m^{-2} is mostly distributed in regions with GDVI greater than 80. This indicates that regions with a lower level of soil moisture have a higher risk of desertification, which corresponds to our existing knowledge of desertification. Soil moisture has a stronger relationship with GDVI than NPP, with most regions having a negative correlation coefficient and being within the 95% confidence level.

3.2 | Risk expansion of global desertification

In order to ensure the future projection, we evaluated CMIP5 simulations of the GDVI compared with observations over the same time period (2000–2014). The results show that the spatial distribution and areal coverage of different risk classes determined by simulation are consistent with observations (Figure 8a,b). Generally, there is a very
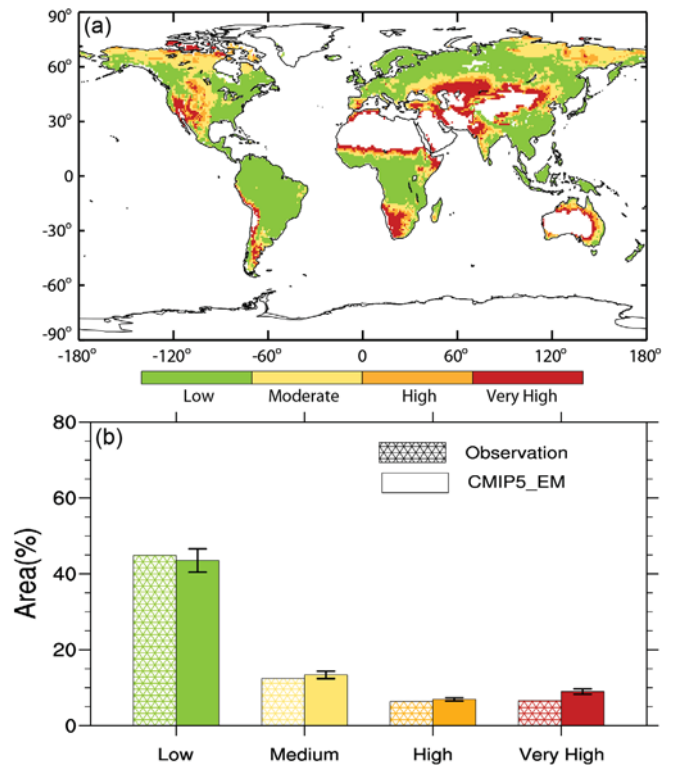

FIGURE 8 (a) The global distribution of desertification risk level during 2000–2014 estimated by the global desertification vulnerability index in the ensemble mean of Fifth Coupled Model Intercomparison Project (CMIP5); (b) The area coverage (percentage of global land area [60°S–65°N]) of different level risk (bar charts filled with an asterisk represent the observed value, and the solid color represents the projected value) [Colour figure can be viewed at wileyonlinelibrary.com]

high risk of desertification in arid and hyperarid areas. Areas with good vegetation cover suffer from lower risk of desertification. There is an area with a difference between the observations and projected values located in northern Canada and eastern Russia. Areas with an observed lower risk of desertification, that is, areas with an overestimation in the ensemble mean of CMIP5 results, are mainly located in western Canada and northern China. However, the observed area coverage of low risk types is greater than the projected area.

Figure 9 shows the evolution of the HAI and LAI from 1981 to 2100. The global mean HAI increases monotonously under the RCP8.5, indicating that human activity would increase in the future. However, under the RCP4.5, the HAI will reach a maximum around 2040 and then decline. The global mean LAI will increase slowly under both the RCP4.5 and RCP8.5, but the rate of increase under RCP4.5 will be lower than that under RCP8.5. The global mean AI values will decrease in the future projection (Huang et al., 2016), and the temperature will increase under both the RCP4.5 and RCP8.5 (Rogelj et al., 2012).

The spatial and temporal distributions of the future desertification risk according to GDVI were presented in Figures 10 and 11. By the end of this century, the coverage of low risk areas will rapidly decline from 47% to 24% under the RCP8.5 and decline to 35% under the
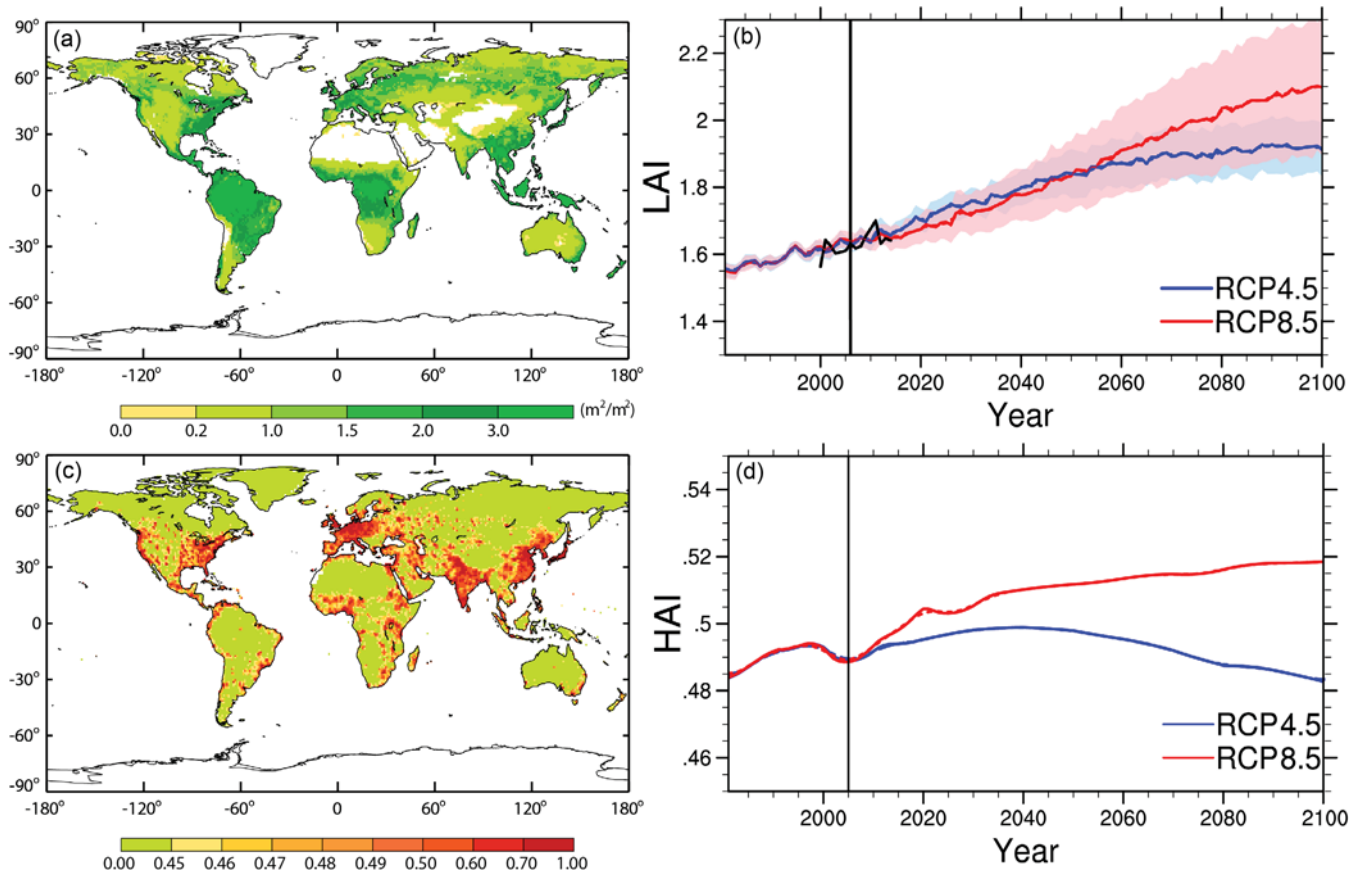
FIGURE 9 (a, c) The observed global distribution of leaf area index (LAI) and human activity index (HAI) for 2000 to 2014. (b, d) The evolution of global averaged LAI and HAI from 1981–2100; the black line (from 2000 to 2014) in (b) is the observed LAI, the blue line represents the representative concentration pathway (RCP) 4.5, the red line represents RCP8.5, and the shading denotes the 95% confidence intervals. Because HAI data were calculated for only one data set, the confidence interval could not be presented here [Colour figure can be viewed at wileyonlinelibrary.com]

RCP4.5 (Figure 11a). The area of moderate, high, and very high risk areas will increase by 10%, 5%, and 8% (Figure 11b–d)), respectively, indicating that the risk of desertification will increase at the global scale under the RCP8.5. Under the RCP4.5, the area of all risk categories, except the low-level risk, will increase slightly by 2100. For the RCP4.5, comparing the means of 2001–2014 and 2086–2100, the risk of desertification according to the GDVI will increase over Europe, western Asia, northern China, the edge of the Sahel, and Mexico (Figure 10a). However, the risk of desertification decreases in the Qinghai–Tibet Plateau and India. The AI decreases and surface air temperature and HAI both increase, which indicate that climate change and human activity both contribute to the increased desertification risk in Europe and western Asia. The HAI decreases over India, resulting in a reduction in desertification risk. HAI also decreases in northern China and at the edge of the Sahel; however, the AI decreases and surface air temperature increases, indicating that climate change dominates the desertification risk increase there. The desertification risk decreases in the Qinghai–Tibet Plateau due to both weakening in human activity and an increase in AI. Under the RCP8.5, HAI increases significantly, the climate becomes drier, and the surface air temperature increases, resulting in a dramatic increase in desertification risk over northern China, India, Mexico, and Europe

(Figure 10b). However, in Australia, climate change is the main contributor to the increased risk of desertification. Although the vegetation coverage increases with the temperature at high latitudes, a drier climate and stronger human activity aggravate the desertification risk.

4 | DISCUSSION

4.1 | The reliability of GDVI

GDVI was constructed by combining the effects of climate change, human activities, and vegetation conditions (Figure 1). Vegetation cover and the AI are important factors in desertification risk estimation (Jafari & Bakhshandehmehr, 2016; Lavado Contador et al., 2009). ΔT is widely used to estimate recent climate change (Dodd et al., 2014). Increasing PD adds pressure to economic and environmental systems. GDP and CO_2 emissions are closely related to economic and social development. Therefore, to estimate the contribution of human activity to global desertification, we combined the effects of PD, GDP, and CO_2 emissions using a weighted scale. The desertification vulnerability map (Figure 4) of USDA (Eswaran & Reich, 2003) was used to verify the result of classified GDVI on the basis of the
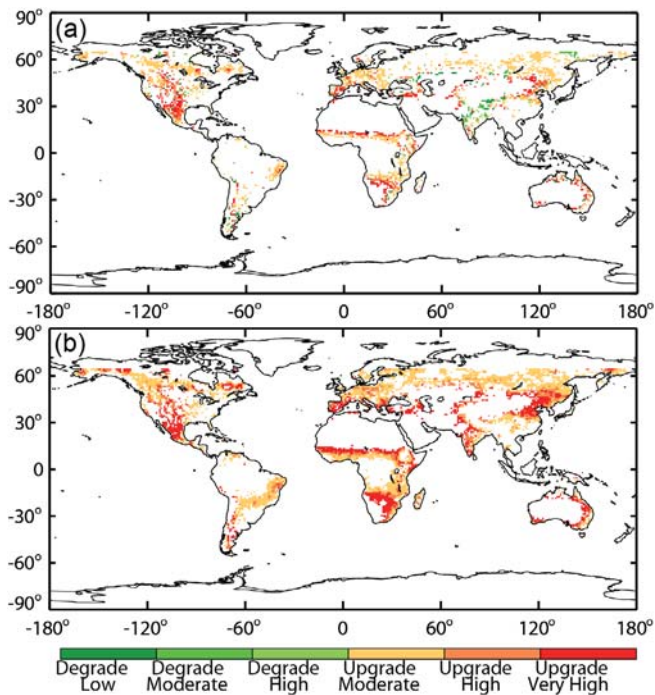
FIGURE 10 The change of desertification risk level in 2086–2100 compared with 2000–2014 under the representative concentration pathway (RCP) 4.5 and RCP8.5. (a) 2081–2100 under the RCP4.5 and (b) 2086–2100 under the RCP8.5. "Upgrade" means indicated risk level transitioned from lower to higher subtypes; and "Degrade" refers to transitioned from original subtypes to a lower risk level [Colour figure can be viewed at wileyonlinelibrary.com]

probability density function (Figure 3). In most regions, the desertification vulnerability maps were coincident (Figure 4). The GDVI's ability to assess global desertification vulnerability was also tested by comparing it with NPP and soil moisture (Figures 5, 6, and 7). Areas with a high GDVI value are sparsely vegetated areas with low levels of NPP (Figures 5 and 6) and dry areas with small amounts of soil moisture (Figures 5 and 7). GDVI was negatively correlated with NPP and soil moisture, both spatially and temporally (Figures 6 and 7). Generally, GDVI produced reasonable and reliable desertification vulnerability results.

4.2 | The distribution of GDVI

According to the GDVI distribution, areas with the highest risk of desertification are mainly located in northern China, northern Africa, western America, India, and Mexico during 2000–2014 (Figure 4). In northern China, desertification was affected by climatic aridity and land use and management, in which socioeconomic factors were predominant (Chen & Tang, 2005; Feng et al., 2015); this is consistent with our results that show that the areas of northern China suffer from more severe desertification risk due to high human activity (Figure 2d) and climatic aridity (Figure 2b). We showed that India suffers from high desertification. Similarly, land degradation in India was

emphasized in Arya et al. (2009) and Kundu et al. (2017). In central Asia, Zhang et al. (2018) showed exacerbated grassland degradation and desertification from 2000 to 2014. Our results also showed that central Asia has a high desertification risk. The high desertification risk and land degradation over Mexico and the Sahel in our study are also reported in the literature (Nicholson et al., 1998; Hein & De Ridder, 2006; Becerril-Piña et al., 2015). However, there are several regions in which our desertification assessment does not agree with previous studies. For example, Tomasella et al. (2018) found that northeastern Brazil suffers from desertification, whereas our results indicated a moderate risk of desertification over this area due to high LAI (Figure 2a) and small ΔT (Figure 2c). Generally, our constructed GDVI works well compared with previous studies in assessing desertification risk.

4.3 | The projection of GDVI

Our results demonstrated that CMIP5 satisfactorily reproduced the spatial distribution of GDVI compared with observations (Figure 8). RCP4.5 assumes the imposition of emissions mitigation policies (Thomson et al., 2011). RCP8.5 is based on a scenario that combines assumptions about high population and relatively slow income growth with modest rates of technological change and energy intensity improvements, leading in the long term to high energy demand and greenhouse gas emissions in the absence of climate change policies (Riahi et al., 2011). Under different policies, human activities will be more intense under the RCP8.5 than under the RCP4.5 (Figure 9), and climate change will be more severe. Under the RCP8.5, low-risk areas will rapidly decline (Figure 11) as high-risk areas largely expand (Figure 10). Subtype changes will be more significant under the RCP8.5 than under the RCP4.5 (Figures 10 and 11). Therefore, a global action plan should be developed to prevent future desertification. It should be noted that uncertainties related to climate change and human activity are expected to increase over time; thus, uncertainty associated with projected GDVI will also increase, despite our use of the multimodel ensemble mean of CMIP5 to reduce the uncertainty of future projections.

4.4 | The weakness of GDVI

Although GDVI provides a picture of risk state combining the influence of climate change, human activities, and vegetation conditions and could help to develop strategies for rehabilitation, it has the weakness of an equal weighting for all indices. A detailed analysis of the causes and main factors leading to global desertification vulnerability was not conducted. With advances in technology and a better understanding of climate change and anthropogenic contributions, ecological protection engineering and rehabilitation technology (Ojeda et al., 2016) are expected to play an increasingly important role in desertification control and mitigation. However, land management and environmental protection depend strongly on the specific region;
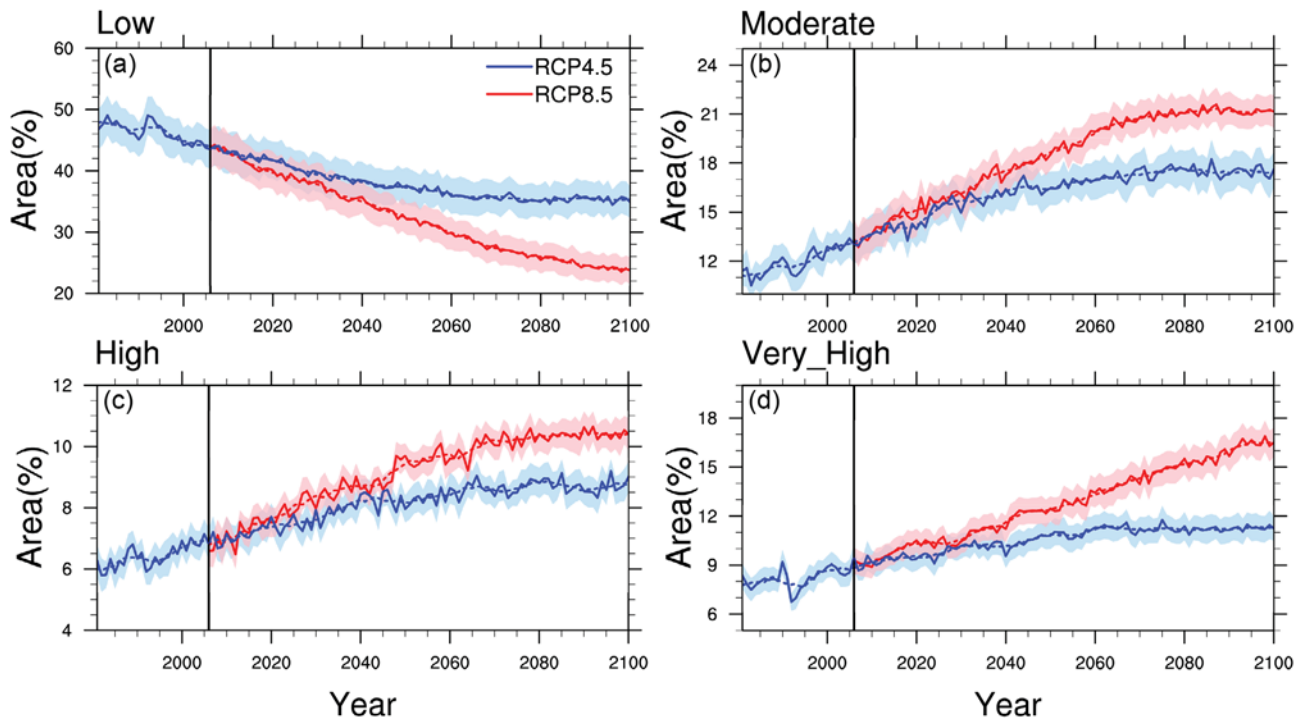
FIGURE 11 The time series of area coverage (percentage of global land area [60°S–65°N]) of different desertification risk from 1981 to 2100. The blue lines represent area under the representative concentration pathway 4.5, the red lines represent the representative concentration pathway 8.5, the shading denotes the 95% confidence intervals. (a) low level, (b) moderate level, (c) high level, and (d) very high level [Colour figure can be viewed at wileyonlinelibrary.com]

thus, it is difficult to quantify their roles in mitigating risk, especially on the global scale. So environmental protection engineering was not quantified in the HAI in this study. As such, our results may overestimate the desertification risk in areas where environmental protection engineering has been implemented. In future studies, the use of the GDVI in a particular local region needs to be carefully verified on the basis of comprehensive local data. Studies are also needed to clarify the contributions of these factors and determine the dominant indicators and subindicators. For the future development of the GDVI, biophysical and socioeconomic factors, such as soil quality, environmental protection engineering, and industrial structure, should be considered to obtain more details of desertification at the global scale.

5 | CONCLUSIONS

This study produced a desertification vulnerability map that considers both climate change and human activities at a global scale and indicated the global area of the risk class of desertification. According to the GDVI distribution, our results show that areas around deserts or barren land have the highest risk of desertification, especially in northern China, northern Africa, western America, India, and Mexico during 2000–2014. We also estimated the spatial and temporal variation of the GDVI using CMIP5 simulations under the RCP4.5 and the RCP8.5. With the expansion of dryland area, warming, and more intensive human activity, the risk of desertification will increase at the global scale. By the end of this century, the coverage of low-risk desertification areas will rapidly decline from 47% to 24% under the RCP8.5 and decrease to 35% under the RCP4.5. There will be an increased risk in North America, eastern Russia, Africa, and northern China. As the area of high-risk desertification expands in the future, poor people in dryland areas will experience more natural disasters, and a global plan of action is therefore needed to reduce the risk of desertification.

ORCID

Jianping Huang https://orcid.org/0000-0003-2845-797X

REFERENCES

Arya, A. S., Ajai, Dhinwa, P. S., Pathan, S. K., & Raj, K. G. (2009). Desertification/land degradation status mapping of India. *Current Science*, 97(10), 1478–1483.

Becerril-Piña, R., Mastachi-Loza, C. A., González-Sosa, E., Díaz-Delgado, C., & Bâ, K. M. (2015). Assessing desertification risk in the semi-arid highlands of central Mexico. *Journal of Arid Environments*, 120, 4–13. https://doi.org/10.1016/j.jaridenv.2015.04.006

Brandt, C. J., & Thornes, J. B. (1996). Mediterranean desertification and land use. *Geographical Journal*, 170(1), 493–495. https://doi.org/10.1007/3-540-58476-5_174

Chen, Y., & Tang, H. (2005). Desertification in north China: Background, anthropogenic impacts and failures in combating it. *Land Degradation & Development*, 16, 367–376. https://doi.org/10.1002/ldr.667

Cherlet, M., Hutchinson, C., Reynolds, J., Hill, J., Sommer, S., & Von Maltitz, G. (2018). *World atlas of desertification*. Luxembourg: Publication Office of the European Union.

Diakoulaki, D., Mavrotas, G., & Papayannakis, L. (1995). Determining objective weights in multiple criteria problems: The CRITIC method. *Computers & Operations Research*, 22(7), 763–770. https://doi.org/10.1016/0305-0548(94)00059-H

Dodd, E. M. A., Merchant, C. J., Rayner, N. A., & Morice, C. P. (2014). An investigation into the impact of using various techniques to estimate Arctic surface air temperature anomalies. *Journal of Climate*, 28(5), 1743–1763. https://doi.org/10.1175/JCLI-D-14-00250.1

Eswaran, H., & Reich, P. (2003). Global desertification vulnerability map. Retrieved from http://www.nrcs.usda.gov/wps/portal/nrcs/detail/soils/use/?cid=nrcs142p2_054003.

Eswaran, H., Reich, P., Vearasilp, T., Faz Cano, A., Mermut, A. R., Arocena, J. M., & Ortiz Silla, R. (2009). Perspectives on desertification during the Anthropocene. Cartagena, Murcia, Spain: Fourth International Conference on Land Degradation (pp. 1–16 ref. 33).

Feng, Q., Ma, H., Jiang, X., Wang, X., & Cao, S. (2015). What has caused desertification in China? *Scientific Reports*, 5, 15998. https://doi.org/10.1038/srep15998

Food and Agriculture Organization of the United Nations. (1977). *World map of desertification*. Rome: FAO.

Geist, H. J., & Lambin, E. F. (2004). Dynamic causal patterns of desertification. *AIBS Bulletin*, 54(9), 817–829. https://doi.org/10.1641/0006-3568(2004)054[0817:DCPOD]2.0.CO;2

Global Land Project. (2005). Global Land Project-Science Plan and Implementation Strategy, IGBP (International Geosphere Biosphere Program) Report No. 53/International Human Dimensions Programme Report No. 19, IGBP Secretariat, Stockholm. Retrieved from www.globallandproject.org/documents.shtml.

Hein, L., & De Ridder, N. (2006). Desertification in the Sahel: A reinterpretation. *Global Change Biology*, 12(5), 751–758. https://doi.org/10.1111/j.1365-2486.2006.01135.x

Henderson-Sellers, A., Irannejad, P., & Mcguffie, K. (2008). Future desertification and climate change: The need for land-surface system evaluation improvement. *Global & Planetary Change*, 64(3), 129–138. https://doi.org/10.1016/j.gloplacha.2008.06.007

Higginbottom, P. T., & Symeonakis, E. (2014). Assessing land degradation and desertification using vegetation index data: Current frameworks and future directions. *Remote Sensing*, 6(10), 9552–9575. https://doi.org/10.3390/rs6109552

Huang, J., Li, Y., Fu, C., Chen, F., Fu, Q., Dai, A., & Wang, G. (2017). Dryland climate change: Recent progress and challenges. *Reviews of Geophysics*, 55(3), 719–778. https://doi.org/10.1002/2016RG000550

Huang, J., Ma, J., Guan, X., Li, Y., & He, Y. (2019). Progress in semi-arid climate change studies in China. *Advances in Atmospheric Sciences*, 36(9), 922–937. https://doi.org/10.1007/s00376-018-8200-9

Huang, J., Yu, H., Guan, X., Wang, G., & Guo, R. (2016). Accelerated dryland expansion under climate change. *Nature Climate Change*, 6(2), 166–172. https://doi.org/10.1038/nclimate2837

Jafari, R., & Bakhshandehmehr, L. (2016). Quantitative mapping and assessment of environmentally sensitive areas to desertification in central Iran. *Land Degradation & Development*, 27, 108–119. https://doi.org/10.1002/ldr.2227

Kosmas, C., Ferrara, A., Briasouli, H., & Imeson, A. (1999). Methodology for mapping environmentally sensitive areas (ESAs) to desertification. In C. Kosmas, M. Kirkby, & N. Geeson (Eds.), *The MEDALUS project: Mediterranean desertification and land use manual on key indicators of desertification and mapping environmentally sensitive areas to desertification* (pp. 31–47). Brussels: European Union.

Kundu, A., Patel, N. R., Saha, S. K., & Dutta, D. (2017). Desertification in western Rajasthan (India): An assessment using remote sensing derived rain-use efficiency and residual trend methods. *Natural Hazards*, 86(1), 297–313. https://doi.org/10.1007/s11069-016-2689-y

Lavado Contador, J. F., Schnabel, S., Gutiérrez, A. G., & Fernández, M. P. (2009). Mapping sensitivity to land degradation in Extremadura SW Spain. *Land Degradation & Development*, 20(2), 129–144. https://doi.org/10.1002/ldr.884

Le Houérou, H. N. (1996). Climate change, drought and desertification. *Journal of Arid Environments*, 34(2), 133–185. https://doi.org/10.1006/jare.1996.0099

Martínez-Valderrama, J., Ibáñez, J., Del Barrio, G., Sanjuán, M. E., Alcalá, F. J., Martínez-Vicente, S., & Puigdefábregas, J. (2016). Present and future of desertification in Spain: Implementation of a surveillance system to prevent land degradation. *Science of the Total Environment*, 563-564, 169–178. https://doi.org/10.1016/j.scitotenv.2016.04.065

Miao, L., Ye, P., He, B., Chen, L., & Cui, X. (2015). Future climate impact on the desertification in the dry land Asia using AVHRR GIMMS NDVI3g data. *Remote Sensing*, 7(4), 3863–3877. https://doi.org/10.3390/rs70403863

Millennium Ecosystem Assessment (MEA). (2005). *Ecosystems and human well-being: Desertification synthesis*. Washington, DC: World Resources Institute.

Nicholson, N. E. (2002). What are the key components of climate as a driver of desertification? In J. F. Reynolds & D. M. Stafford Smith (Eds.), *Global desertification: Do humans cause deserts?* Berlin: Dahlem University Press.

Nicholson, S. E., Tucker, C. J., & Ba, M. B. (1998). Desertification, drought, and surface vegetation: An example from the West African Sahel. *Bulletin of the American Meteorological Society*, 79(5), 815–830. https://doi.org/10.1175/1520-0477(1998)079<0815:DDASVA> 2.0.CO;2

Ojeda, G., Patrício, J., Mattana, S., & Sobral, A. J. F. N. (2016). Effects of biochar addition to estuarine sediments. *Journal of Soils and Sediments*, 16(10), 2482–2491. https://doi.org/10.1007/s11368-016-1493-3

Pravalie, R., Savulescu, I., Patriche, C., Dumitrascu, M., & Bandoc, G. (2017). Spatial assessment of land degradation sensitive areas in southwestern Romania using modified MEDALUS method. *Catena*, 153, 114–130. https://doi.org/10.1016/j.catena.2017.02.011

Qi, F., Wei, L., & Xi, H. (2013). Comprehensive evaluation and indicator system of land desertification in the Heihe River Basin. *Natural Hazards*, 65(3), 1573–1588. https://doi.org/10.1007/s11069-012-0429-5

Rampone, S., & Valente, A. (2019). Assessment of desertification vulnerability using soft computing methods. *Journal of Ambient Intelligence and Humanized Computing*, 10(2), 701–707. https://doi.org/10.1007/s12652-018-0720-8

Reynolds, J. F., Smith, D. M. S., Lambin, E. F., Turner, B., Mortimore, M., Batterbury, S. P., & Herrick, J. E. (2007). Global desertification: Building a science for dryland development. *Science*, 316(5826), 847–851. https://doi.org/10.1126/science.1131634

Riahi, K., Rao, S., Krey, V., Cho, C., Chirkov, V., Fischer, G., & Rafaj, P. (2011). RCP8.5—A scenario of comparatively high greenhouse gas emissions. *Climatic Change*, 109(1), 33–57. https://doi.org/10.1007/s10584-011-0149-y

Rogelj, J., Meinshausen, M., & Knutti, R. (2012). Global warming under old and new scenarios using IPCC climate sensitivity range estimates.

Nature Climate Change, *2*(4), 248–253. https://doi.org/10.1038/nclimate1385

Shinoda, M., & Nandintsetseg, B. (2011). Soil moisture and vegetation memories in a cold, arid climate. *Global & Planetary Change*, *79*(1), 110–117. https://doi.org/10.1016/j.gloplacha.2011.08.005

Sivakumar, M. V. K. (2007). Interactions between climate and desertification. *Agricultural and Forest Meteorology*, *142*(2), 143–155. https://doi.org/10.1016/j.agrformet.2006.03.025

Spinoni, J., Vogt, J., Naumann, G., Carrao, H., & Barbosa, P. (2015). Towards identifying areas at climatological risk of desertification using the Köppen–Geiger classification and FAO aridity index. *International Journal of Climatology*, *35*(9), 2210–2222. https://doi.org/10.1002/joc.4124

Stafford Smith, D. M., & Reynolds, J. F. (2002). Desertification: A new paradigm for an old problem. In J. F. Reynolds & D. M. Stafford Smith (Eds.), *Global desertification: Do humans cause deserts? Dahlem workshop report 88*. Berlin: Dahlem University Press.

Symeonakis, E., Karathanasis, N., Koukoulas, S., & Panagopoulos, G. (2016). Monitoring sensitivity to land degradation and desertification with the environmentally sensitive area index: The case of Lesvos Island. *Land Degradation & Development*, *27*(6), 1562–1573. https://doi.org/10.1002/ldr.2285

Thomson, A. M., Calvin, K. V., Smith, S. J., Kyle, G. P., Volke, A., Patel, P., & Edmonds, J. A. (2011). RCP4.5: A pathway for stabilization of radiative forcing by 2100. *Climatic Change*, *109*(1), 77–94. https://doi.org/10.1007/s10584-011-0151-4

Tomasella, J., Silva Pinto Vieira, R. M., Barbosa, A. A., Rodriguez, D. A., Oliveira Santana, M. D., & Sestini, M. F. (2018). Desertification trends in the northeast of Brazil over the period 2000–2016. *International Journal of Applied Earth Observation and Geoinformation*, *73*, 197–206. https://doi.org/10.1016/j.jag.2018.06.012

UNCCD, 1994. United Nations convention to combat desertification in countries experiencing serious drought and/or desertification, particularly in Africa. A/AC.241/27, Paris.

Verstraete, M. M., Scholes, R. J., & Smith, M. S. (2009). Climate and desertification: Looking at an old problem through new lenses. *Frontiers in Ecology and the Environment*, *7*(8), 421–428. https://doi.org/10.1890/080119

Yassoglou, N. J., & Kosmas, C. (2000). Desertification in the Mediterranean Europe. A case in Greece. In RALA Report (pp 27–33), Reykjavik, Iceland: CiteSeer[x]

Yu, P., Han, D., Liu, S., Wen, X., Huang, Y., & Jia, H. (2018). Soil quality assessment under different land uses in an alpine grassland. *Catena*, *171*, 280–287. https://doi.org/10.1016/j.catena.2018.07.021

Zhang, G., Biradar, C. M., Xiao, X., Dong, J., Zhou, Y., Qin, Y., & Thomas, R. J. (2018). Exacerbated grassland degradation and desertification in Central Asia during 2000–2014. *Ecological Applications*, *28*(2), 442–456. https://doi.org/10.1002/eap.1660

Zhang, Y., Huang, J., Guan, X., & Guo, R. (2017). Quantitative assessment of global human activity's influence on climate. *Journal of Arid Meteorology* (In Chinese), *35*(2), 182–189. Doi: https://doi.org/10.11755/j.issn.1006-7639(2017)-02–0182.

SUPPORTING INFORMATION

Additional supporting information may be found online in the Supporting Information section at the end of this article.